Assessment of Short-medium Term Intervention Effects Using CAESAR-Lisflood in Post-earthquake Mountainous Area

Di Wang[1,2,3], Ming Wang[1], Kai Liu[1], Jun Xie[1]

[1]School of National Safety and Emergency Management, Beijing Normal University, Beijing, China.

[2]Academy of Disaster Reduction and Emergency Management, Beijing Normal University, Beijing, China.

[3]Faculty of Geographical Science, Beijing Normal University, Beijing, China.

Correspondence to: Ming Wang (wangming@bnu.edu.cn)

Abstract. The 2008 Wenchuan earthquake triggered local geomorphic changes rapidly, producing abundant material through exogenic processes. The substantial material dynamics increased the risks of geo-hazards (flash floods, landslides, and debris flows) induced by extreme precipitation in the area. Intervention measures such as dams, levees, and vegetation revetments have been constructed in specified sites to reduce sediment transport, thus mitigating the risk of ensuing geo-hazards.
This study focused on assessing intervention effects incorporated with various facilities on post-earthquake fragile mountains in the short-medium term. Taking the Xingping valley as an example, we used the CAESAR-Lisflood, a two-dimensional landscape evolution model, to simulate three scenarios: unprotected landscapes, present protected landscapes, and enhanced protected landscapes between 2011 and 2013. We defined two indicators to assess the intervention effects of the three scenarios by comparing the geomorphic changes and sediment yield.
The results showed that the mitigation facilities were effective, especially engineering efforts cooperating with vegetation revetments in the upstream area. The spatial patterns of erosion and deposition changed considerably caused of the intervention measures. Additionally, the effectiveness of each intervention scenario showed a gradual decline caused directly by the reduction of the reservoir capacity. The enhanced scenario functioned better than the present one, with a smaller downward trend. The simulation results assessed the ability and effectiveness of cooperated control measures and could support optimum mitigation strategies.

1 Introduction

Strong earthquakes trigger co-seismic landslides and crack the mountains discontinuously, increasing weak structural planes (Huang, 2009) by weathering and erosion. Consequently, the source material produced from co-seismic landslides and attendant mass failure caused by the weak slope increase in mountainous regions and modify mountain landscapes by various surface processes for days, years, and millennia (Fan et al., 2020). The 2008 Wenchuan Ms 8.0 (the surface-wave magnitude, which is the logarithm of the maximum amplitude of ground motion for surface waves with a wave period of 20 seconds) earthquake has been influencing towns and other infrastructure in the affected area. Many studies have mapped the landslides triggered by the devastating earthquake. Gorum et al. (2011) performed an extensive landslide interpretation using a large set of high-resolution optical images and mapped nearly 60000 individual landslides, which are no less than 600 m^2. Xu et al. (2014) delineated 197481 landslides formed by polygons, centroids, and top points compiled from visual image interpretation. To estimate the threat of loose material in subsequent sediment disasters caused by landslides, some research attempt to measure the volume of deposited material based on field survey and assumptions. Huang and Fan (2013) estimated 400 million m^3 of material deposited in the heavy-affected areas by assuming that the material deposited on steep slopes with angles larger than 30° and a catchment area of more than 0.1 km^2. An approximate 2793 million m^3 of sediment was calculated by Chen et al. (2009) using different deposited depth settings in different buffer zones of the Longmenshan central fault. In summary, a tremendous number of loose material accumulated on the gullies and hillslopes, ready to be eroded and transported away over a long time. As a result, the mitigation in the Wenchuan quake-stricken area is still in the long run.

Structural mitigation measures have been developed in the affected areas regarding the site conditions and technical and economic feasibilities. For example, ecological mitigation such as vegetation revetments was conducted to stabilise the source area in hillslopes (Cui and Lin, 2013; Forbes and Broadhead, 2013; Stokes et al., 2014), and check dams were used widely to intercept upriver sediment (Yang et al., 2021; Marchi et al., 2019). Lateral walls and levees were the longitude structures (Marchi et al., 2019) to protect the infrastructures in mountain watersheds with higher sediment supply to the main streams.

Although comprehensive mitigation measures were performed in potentially dangerous sites, disasters still occurred owing to rough terrain, vague source material, intensive precipitation, and relatively low-cost mitigating measures (Yu et al., 2010; Cui et al., 2013). Therefore, understanding the effectiveness of intervention measures is crucial for mitigation strategies. Some studies mainly focus on establishing post-evaluation effectiveness index systems that are not supported by sufficient practices (Zhang and Liang, 2005; Wang et al., 2015). Some researchers compare the changes before and after the intervention measures recorded by the long-term on-site measurement, which face the challenges to the investment of much time, energy and financing (Zhou et al., 2012; Chen et al., 2013). Recent research compares the disaster characteristics before and after the mitigation actions, which are quickly obtained from the numerical simulation (Cong et al., 2019; He et al., 2022). Nevertheless, these disaster characteristics express the process ignoring the long-time effects on the geomorphic changes (longer than the duration of a single event). Therefore, the short-medium term (from the duration to decades) and spatial geomorphic changes quickly obtained from the simulation will provide more details to interpret engineering measures in notable locations, even in those inaccessible to humans.

CAESAR-Lisflood (C-L), which is based on the Cellular Automata (CA) framework (Coulthard et al., 2013), has powerful spatial modelling and computing capabilities to simulate complex dynamic systems(Batty and Xie, 1997; Couclelis, 1997; Coulthard et al., 2002). The model enables the study of many earth system interactions under different geo-environmental. Representation of deposition and erosion within C-L is used widely in rehabilitation planning and soil erosion predictions from a post-mining landform (Saynor et al., 2019; Hancock et al., 2017; J.B.C. Lowry et al., 2019; Thomson and Chandler, 2019; Slingerland et al., 2019) and channel evolution and sedimentary budget with dam settings (Poeppl et al., 2019; Gioia and Schiattarella, 2020; Ramirez et al., 2020, 2022). In addition, there were a series of studies in the mountainous area involving secondary geo-hazard driving factors (Li et al., 2018; Wang et al., 2014b) and vegetation recovery (Zhang et al., 2018). Li et al. (2020) and Xie et al. (2018) have used C-L with different rainfall scenarios or future climate change to interpret the landscape evolution after the Wenchuan earthquake. The methods and parameter values used in the above research helped to promote the application in other study areas.

In this study, the hourly rainfall data of three years was generated by downscaling from daily to capture the extreme event. Based on the input data, we simulated and compared the geomorphic changes and sediment yield in three scenarios that varied in mitigation compositions and intensities in a catchment. The objectives are to 1) assess the effectiveness of a set of mitigation facilities to reduce sediment transport, 2) analyse the role of each facility on geomorphic changes, and 3) determine vegetation influence on catchment erosion.

2 Study area

2.1 Regional characteristics

The study area was Xingping valley in the northeastern Sichuan province, a left branch of the Shikan river (a tributary of the Fu River) (Fig. 1). There are nearly two hundred households scattered among more than five villages in the catchment. The topography of the catchment is rugged, with an elevation between 800 and 3036 m and an area of approximately 14 km^2. The catchment is characterised by a high longitudinal gradient (~ 120‰) and more than ten small V-shaped branch gullies. The length from northeast to southwest is 5770 m, the other direction perpendicular to which is 4150 m. A humid temperate climate with a mean annual temperature of 14.7℃ characterises the region. The mean annual precipitation is 807.6 mm, mainly concentrated between May and September. The steep terrain and short-term heavy rainfall make an ephemeral stream in this area. The local basement rocks are mainly metamorphic sandstones, sandy slate, crystalline limestone, and phyllite of Triassic Xikang Group (T_{3xk}) and Silurian Maoxian Group (S_{mx}), which are easily worn away by quickly weathering in a static process after disturbed in a strong earthquake. Consequently, the Wenchuan earthquake, with a Modified Mercalli Intensity scale of X, made this area one of the most severely affected locations (Wang et al., 2014a) and produced 10^6 m^3 loose material by triggering landslides and subsequent weathering in Mayuanzi, Zhengjiashan, and Wujiaping (Fig. 1)(Guo et al., 2018).

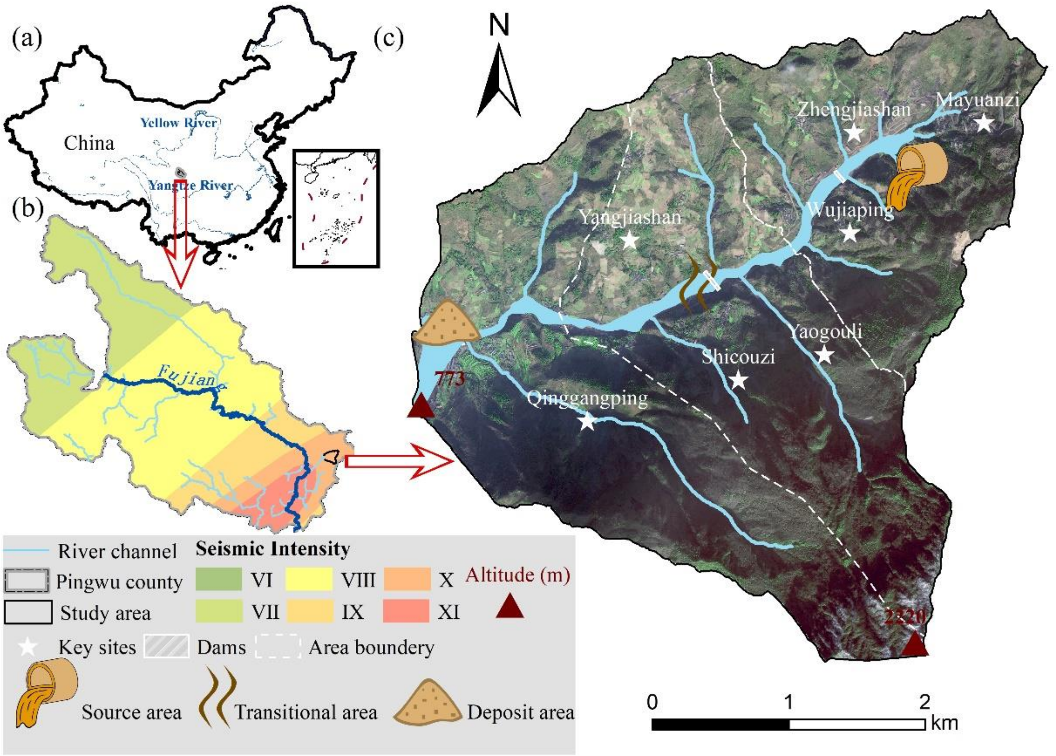

Figure 1: Overview of the study area. (a) Location of study area; (b) Seismic intensity map of the Wenchuan earthquake within the Pingwu county; (c) The schematic image of the study area.

2.2 Historical hazards and intervention measures

Six group debris flow-flash flood disaster chains have been found in Xingping valley over a decade after the earthquake. Based on the published work of SKLGP (State Key Laboratory of Geohazard Prevention and Geoenvironment Protection) and the local states' geological survey before 2018 and our biannual field surveys since 2012, we catalogued the time of occurrence, total rainfall of each event, corresponding disaster details (Table S1). The massive sediment was transported quickly after the devastating quake in 2008 and 2009, and the extreme rainfall in 2013 and 2018 triggered prosperous loose material deposited in the channel. Considering the landslide processes, we divided the study area into three regions: source area, transitional area, and deposit area (the white dashed lines in Fig. 1c), which means the loose solid material would be easily transported from the source area to the deposit one through the transitional zone.

An engineering control project was constructed to intercept the upriver material in October 2010. The project included two check dams, one in the upper source area and the other in the transitional zone (Feng et al., 2017) (Fig. 1c). The upper dam has a storage capacity of 5.78×10^4 m^3 and a height of 10.0 m. The transitional area dam has a storage capacity of 7.2×10^4 m^3 and a height of 9.0 m. With the reservoirs gradually filling with deposits, the first dredging work was subsequently done in

2013. Nearly three years later, the storage capacity behind the upper dam remained at 50% in 2016, while the transitional area dam can no longer retain sediment.

3 Materials and Methods

In this study, we examined the intervention effectiveness through the morphological response and sediment yield in the Xing-ping valley, which was simulated using the C-L model. The research entailed four main steps: 1) setting three scenarios with different intervention compositions, 2) preprocessing the model input data, including three groups of DEMs, the rainfall data, and m value of the C-L, 3) calibration of the hydrological component, and 4) simulating landscape changes and analysing the intervention effectiveness in 2011-2013.

3.1 Scenarios settings

The abundant source material triggered by landslides should be controlled to prevent the threat of disasters downstream. Therefore, we designed three scenarios by incorporating engineering and biological measures referenced to current facilities to assess the effectiveness of intervention measures. Scenario UP: Unprotected landscapes meant the sediments would transport without anthropogenic intervention. Scenario PP: Present protected landscapes implied that only the present two check dams trapped deposits in 2011-2013 without dredging work over the period (see section 2.2). Scenario EP: Enhanced protected landscapes emphasised the plus vegetation revetments in the source area and levees in the deposit area based on the two check dams in Scenario PP.

Fig. 1c shows the locations of the existing two check dams in both Scenario PP and Scenario EP. We determined the placements of additional facilities in Scenario EP according to the field survey, which demonstrated that the continuous supply of sediments was mainly from the source area. Therefore, the vegetation revetments like tree planting would be carried out in upstream to prevent erosion by stabilising topsoil and enhancing the soil's infiltration capacity with its roots (Lan et al., 2020).

Considering the damages caused by flash-flood to the residential area downstream, the levees (see Fig. S1 and Section 3.2.2) are artificial barriers to protect agricultural land and buildings, which helped to prevent water and sediment from overflowing and flooding surrounding areas. Table 1 shows the scenario descriptions, initial model conditions and input rainfall series. The details about model input data are introduced below.

Table 1: Scenarios setting

Scenario	Descriptions	Period	DEM (10m)	Rainfall data
UP	no anthropogenic intervention		UP DEM UP bedDEM	downscaled hourly precipitation in the period (lumped)
PP	the present two check dams upstream without dredging work	2011-2013 (3 years)	PP DEM PP bedDEM	
EP	additional vegetation revetments in the source area and levees in the deposit area based on Scenario PP		EP DEM EP bedDEM	downscaled hourly precipitation in the period (spilt)

3.2 CAESAR-Lisflood

The C-L integrated the Lisflood-FP 2D hydrodynamic flow model (Bates et al., 2010) with the CAESAR landscape evolution model (LEM) (Coulthard et al., 2002; Van De Wiel et al., 2007), which is described in detail by Coulthard et al. (2013). The catchment mode of C-L was applied in this study, within which the surface digital elevation model (DEM), the bedrock DEM, the grain size distribution, and a rainfall time series are required to simulate the sediment transport and geomorphic changes. There are four primary modules within C-L operated as follows:

(1) a hydrological module generates surface runoff from rainfall input using an adaption of TOPMODEL (Topography based hydrological model) (Beven and Kirkby, 1979),
(2) a hydrodynamic flow routing module based on the Lisflood-FP method (Bates et al., 2010) calculates the flow depths and velocities,
(3) an erosion and deposition module uses hydrodynamic results to drive fluvial erosion by either the Einstein (1950) or the Wilcock et al. (2003) equation applied to each sediment fraction over nine different grain sizes,
(4) and a slope model moves material from the hillslope to the fluvial system by considering both the mass movement when a critical slope threshold is exceeded, and soil creep processes whereby sediment flux is linearly proportional to surface slope.
The C-L model updates variable values stored in square grid cells at intervals, such as DEM, grain size and proportion data, water depth, and velocity. For three scenarios, the initial conditions, such as DEMs and bedrock DEMs, the rainfall data, and the m values were preprocessed as follows.

3.2.1 Surface and bedrock digital elevation model

To describe clearly the control process, especially the two dams and levees in the catchment, we unified grid cell scales to 10 m for all input data of the C-L. The GlobalDEM product with a 10 m × 10 m resolution and 5 m (absolute) vertical accuracy was used to form three types of initial DEMs (UP DEM, PP DEM, and EP DEM). Before rebuilding initial DEMs, we filled the sinks of the original GlobalDEM based on Environmental Systems Research Institute's (ESRI's) ArcMap (ArcGIS, 10.8) to eliminate the 'walls' and the 'depressions' in the cells and avoided the intense erosion or deposition in the early run time. Then the non-sinks DEM was used as the surface DEM in Scenario UP (UP DEM) without any facilities. According to the engineering control project described in Section 3.2.2, surface DEM of Scenario PP (PP DEM) included the dams by raising the grid cell elevations by 10 m for the dam in upper stream and 9 m for the dam in the transitional area. Similarly, the surface DEM in Scenario EP (EP DEM) included the dams in PP DEM. In addition, two levees were produced by raising grid cells' elevation by 2 m that were represented at selected locations. For scenario EP, the placement and setting of vegetation revetments in Scenario EP were introduced in Section 3.2.2.
The spatial heterogeneity of source material (Fig. 1c) indicates the discrepancy of erodible thickness, which equals the difference between surface DEM (DEM) and bedrock DEM (bedDEM). We divided the study area into five regions according to the erodible thickness (Fig. S1) by checking out the relative elevation of the foundations of buildings, the exposed bedrock, and the deposited depth of landslides to the ground level. The average thicknesses of upstream low and high-altitude areas were set to 10 m and 3 m, respectively, and the thickness of erodible layer in the downstream area was set to 3 m. For the river channel and outlet, there would be a large amount of deposition; the thickness of erodible sediment was set to 5 m and 4 m, respectively. As the dams in Scenario PP and the levees in Scenario EP were non-erosive concrete, we set the erodible thickness of these features to 0 m. Eventually, DEMs were formatted to ASCII raster as required by C-L. The divided regions varied in erodible thickness, the placement of additional levees and vegetable revetments in Scenario EP, and the generation process of DEMs and bedDEMs were shown in Fig. S1.

3.2.2 Vegetation settings

Another parameter required in each scenario simulation was the m value of hydrological model (TOPMODEL) within C-L, which controls the exponential decline of transmissivity with depth (Beven, 1995, 1997) and influences the peak and duration of the hydrograph in response to rainfall. The m value effectively imitates the effect of vegetation on the movement and storage of water within the soil. The lower the m value, the lower the vegetation coverage, and the flashier flood peak and shorter duration are reflected in the flood hydrograph (Coulthard et al., 2002). The m value is usually determined by the landcover (e.g., 0.02 for the forest, 0.005 for the grassland) (Coulthard and Wiel, Van De J., 2017). In our study, we set the m value as

0.008 in our smaller catchment (14 km^2) in Scenario UP and PP, which resembles the m value of farmland covered with lower vegetation coverage in the same catchment studied by Xie et al. (2018) and Li et al. (2018). As mentioned earlier, the upstream-low elevation area covered by the biological measures in the EP scenario was assigned a higher m value of 0.02. It has been calibrated in the more extensive catchment containing our study area by replicating the flood event in 2013 (Xie et al., 2018).

3.2.3 Rainfall data

In this research, we compared three scenarios with identical precipitation data between 2011 and 2013, as mentioned in section 3.1. The source data of precipitation in 2011-2013 (Fig. 2a) was obtained from the China Meteorological Administration (http://data.cma.cn) with daily temporal resolution. The intensity and frequency of extreme rainfall events affect patterns of erosion and deposition (Coulthard et al., 2012b; Coulthard and Skinner, 2016). Therefore, we used the stochastic downscaling method to generate hourly data to better capture the hydrological events introduced by Li et al. (2020) and Lee and Jeong (2014). The referenced hourly precipitation was observed from the pluviometer located 20 km from the study area in 2016 (Fig. 2b), with an annual total precipitation of 684 mm. The observed rainfall in 2016 was characterised by: (1) hourly precipitation was from 1.1 mm to 35.4 mm, and (2) the maximum and average duration of a rainfall event was 24 h and 2.8 h, respectively. The main processes of the downscaling method are:

- extracting the hourly rainfall of specific days in 2016 closest to the daily rainfall in 2011-2013 through the threshold setting and producing the genetic operators using the extracted hourly rainfall dataset;
- mixing on the genetic operators by genetic algorithm (Goldberg, 1989) composed of reproduction, crossover and mutation and repeating until the distance between the sum of hourly rainfall and the actual daily rainfall is less than the set threshold;
- normalising the hourly precipitation to remain the daily rainfall value unchanged.

Fig. 2c shows the downscaled rainfall series between 2011 and 2013. The downscaled hourly rainfall better captured the hydrological events at an hourly scale compared to the hourly-mean rain (5.27 mm) on the day with extreme rainfall (126.5 mm), which was far from the actual situation. Corresponding to the m value settings, the input of generated hourly precipitation is catchment lumped in Scenario UP and Scenario PP and divided into two separate but identical rainfall in Scenario EP.

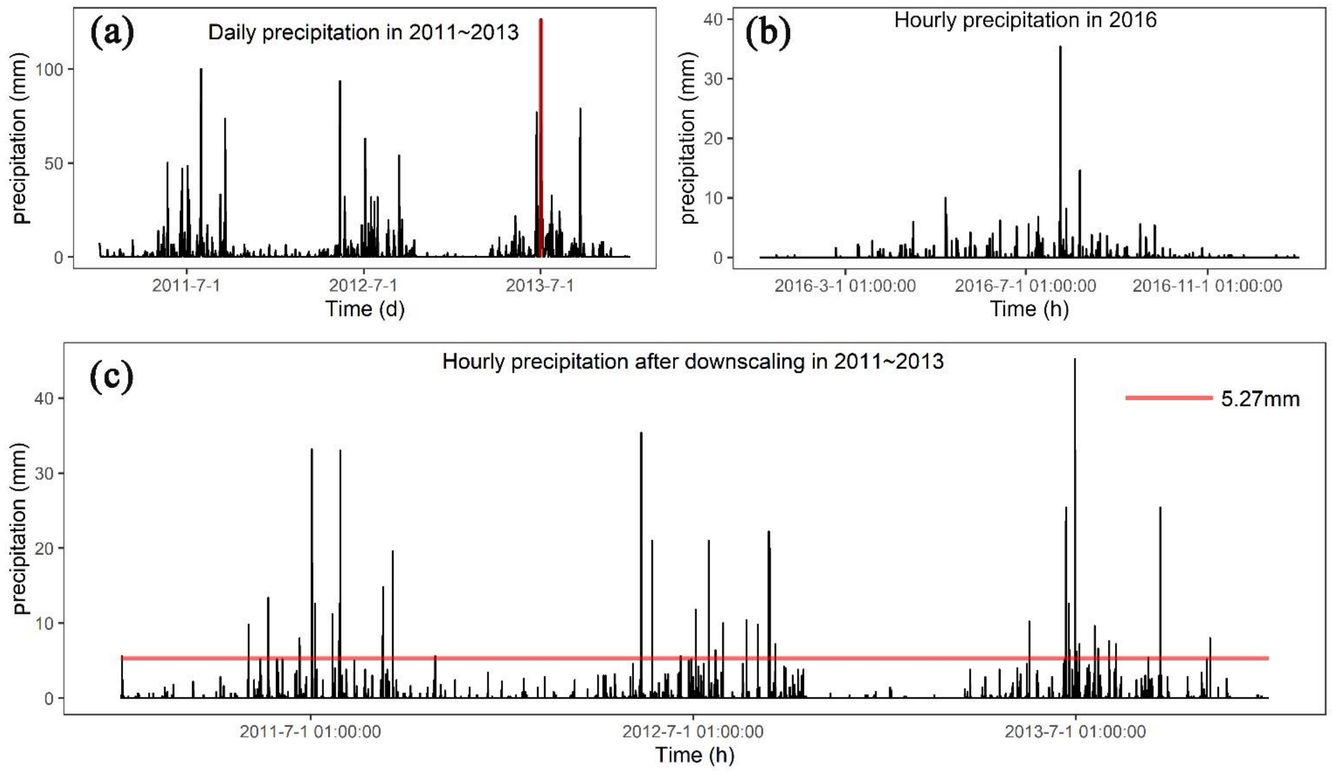

Figure 2: (a) Daily precipitation in 2011-2013 (the red vertical line indicates maximum daily precipitation of 126.5 mm); (b) Hourly precipitation in 2016; (c) Downscaled hourly precipitation in 2011-2013 (the red horizontal line indicates the hourly-mean precipitation 5.27 mm on the day with maximum precipitation marked in (a)).

3.2.4 Other parameters

The C-L is sensitive to a set of input data introduced by Skinner et al. (2018) for a catchment with a grid cell size of 10 m, such as sediment transport formula, slope failure threshold, and grain size set. The grainsize distribution of sediment is derived from samplings at 14 representative locations in the same study basin by Xie et al. (2018). Given the grainsize distribution in this study, the Wilcock and Crowe formula was selected as the sediment transport rule, which was developed from flume experiments using five different sand-gravel mixtures with grain sizes ranging between 0.5 and 64 mm (Wilcock et al., 2003). Considering the steep slope on both sides of deep gullies, a higher slope failure threshold was determined to replicate the geomorphic changes between 2011 and 2013. Additionally, we found that the probability of shallow landslides indeed accumulated from 20°to 50° in slope gradient between 2011 and 2013 (Li et al., 2018). The slope angle was derivate from the DEM with a 30 m spatial resolution, which caused a lower slope angle than that with a 10 m resolution. As such, we set 60°, which is lower than the 65° used in a scenario without landslides (Xie et al., 2022) and higher than 50°. Some parameters were determined by repeated experiments such as the minimum Q value, and the other input values were referred to default values recommended by the developers (such as the max erode limit in the erosion/deposition module and the vegetation critical shear stress) in https://sourceforge.net/p/caesar-lisflood/wiki/Home/. Table S2 in the supplemental material presented model parameters of C-L used in this study.

3.2.5 Model calibration

Considering the ungauged basins before 2015, we replicated the flash flood event in July 2018 using C-L simulations to calibrate the hydrological components. Based on Scenario PP (with two checking dams), we input the two-week hourly precipitation in July 2018 (Fig. S2a), which is recorded by the rain gauge located 2.5 km away from the catchment (Fig. S2b). The simulation results (Fig. S2c and Fig. S2d) show the erosion map and maximum water depth map in Scenario PP on July 15, 2018. We selected three locations to compare the deposition and inundation in simulation results, satellite images and photos (Fig. S3). Additionally, the simulated sediment thickness and water depth were close to those measured from pictures, which indicated that the flash flood event was well replicated by the C-L using the input data.

3.3 Output analysis

The C-L model outputs in each scenario include hourly water and sediment discharge at the basin outlet, the difference between DEMs at a specified time and initial DEMs (EleDiffs). We validated the model outputs by comparing the hourly discharge and EleDiffs reflecting the depth of sediment deposition or erosion (> 0.1 m: deposition, < -0.1 m: erosion) with field survey materials. The overall temporal and spatial geomorphic changes reflected by EleDiffs under three different scenarios were used to assess the geomorphic response to interventions. To explore the geomorphic response to various control measures, we focused on the key spots placed checking dams, levees, and vegetation revetments and recorded the depth of deposited sediment behind two dams. To further explore the spatial heterogeneity, we compared the volumes of deposition and erosion among three divided regions, including the source area, transitional area, and deposition area.

Based on the visual analysis and quantitative results, we defined two formulae to assess the effectiveness of intervention. The conservation ability (*Ca*, Eq. (3)) was calculated based on variables in the sediment balance system (Fig. 3). The sediment volume of deposited sediment (D_n) and input sediment from the upper connected region (I_n) is equal to that of eroded material (E_n) and output sediment to the next part (O_n) over the same period (Eq. (1), Eq. (2)) in the system. A higher value of *Ca* in a specific region and scenario indicates that a more effective control system is applied.

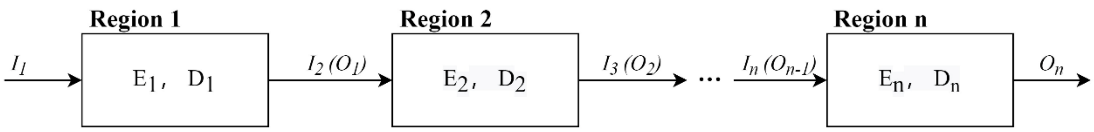

Figure 3: The sediment balance system in the study area (the Region *n* indicated source area, transitional area, and deposit area)

$$I_n = \sum_{2}^{n} E_{n-1} - \sum_{2}^{n} D_{n-1}, \tag{1}$$

$$I_n + E_n = O_n + D_n, \tag{2}$$

$$Ca = \frac{D_n}{I_n + E_n} \tag{3}$$

Where, n is the region number of source area (=1), transitional area (=2), and deposit area (=3).

Additionally, we designed the relative efficiency (Re, Eq. (4)) to depict the efficiency of intervention measures in Scenario PP and EP in sediment loss, with the comparison to Scenario UP.

$$Re_{PP/EP,i} = \frac{Q_{UP,i} - Q_{PP/EP,i}}{Q_{UP,i}} \tag{4}$$

Where i is the sequence of the day; Q_{UP} is the daily sediment yield measured at the catchment outlet in Scenario UP; $Q_{PP/EP}$ is the daily sediment yield measured at the catchment outlet in Scenario PP or Scenario EP of day i; $\mathrm{Re}_{PP/EP}$ is the daily relative effectiveness of control measures in Scenario PP or Scenario EP.

4. Results

4.1 Model verification

Fig. 4 shows the input rainfall data and modelled discharge hydrograph between 2011 and 2013 (Fig. 4a). The comparison of simulated mean discharge in April through July and the whole year with field survey materials in two locations are also presented (Fig. 4b, c). Concerning the discharge hydrograph, the peak discharges (63.7, 54.9, and 50.3 m^3/s) correspond well with the peak rainfall intensities (31, 19.7 and 15 mm). The modelled water discharge from March to May in location A is slightly larger than the measured value reported by Feng et al. (2017). Additionally, an average annual discharge of 10.04 m^3/s in location A is less than that of 12.80 m^3/s in the catchment outlet (location B), which has an area approximately three times the size of the study area.

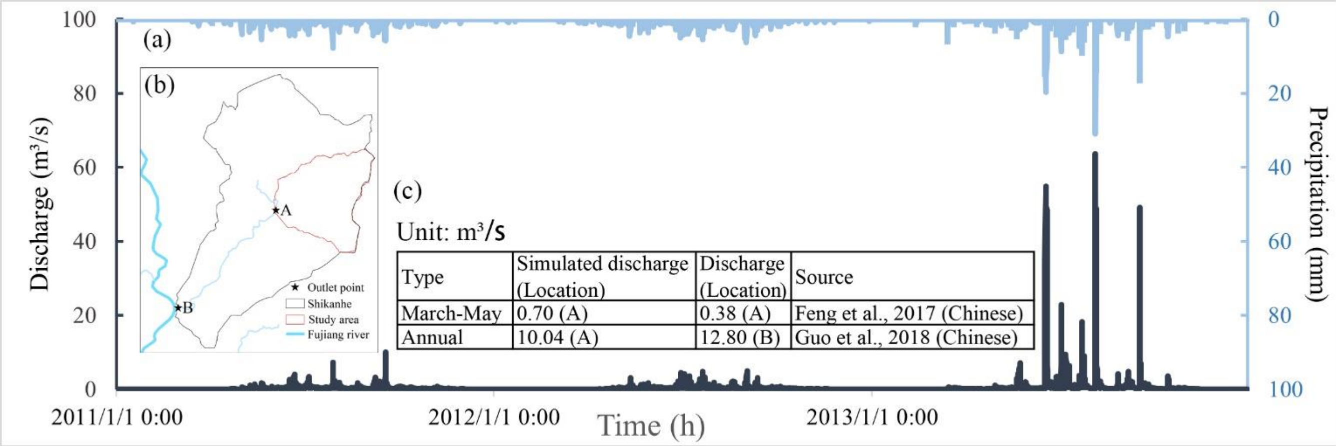

Figure 4: The input and output of the hydrograph. (a) The input hourly precipitation and simulated discharge in 2011-2013 in Scenario PP; (b) Location of the specified outlet point; (c) the comparison of the simulated average discharge to the recorded discharge.

Typical cross-sections are generated (Fig. 5) based on the replicated landscape changes in Scenario PP. The first site is located on the upriver road, which was eroded at a depth of 5.7 m according to the simulation results, while the photo shows a depth of no less than 4.0 m without an apparent eroded base. The cross-section #2 and site photo of the gully depict that the eroded depth is approximately 1.0 m. Meanwhile, a clear sediment boundary is found in the building located at the deposited area (# 3), indicating a slightly lower deposition depth than the modelled one.

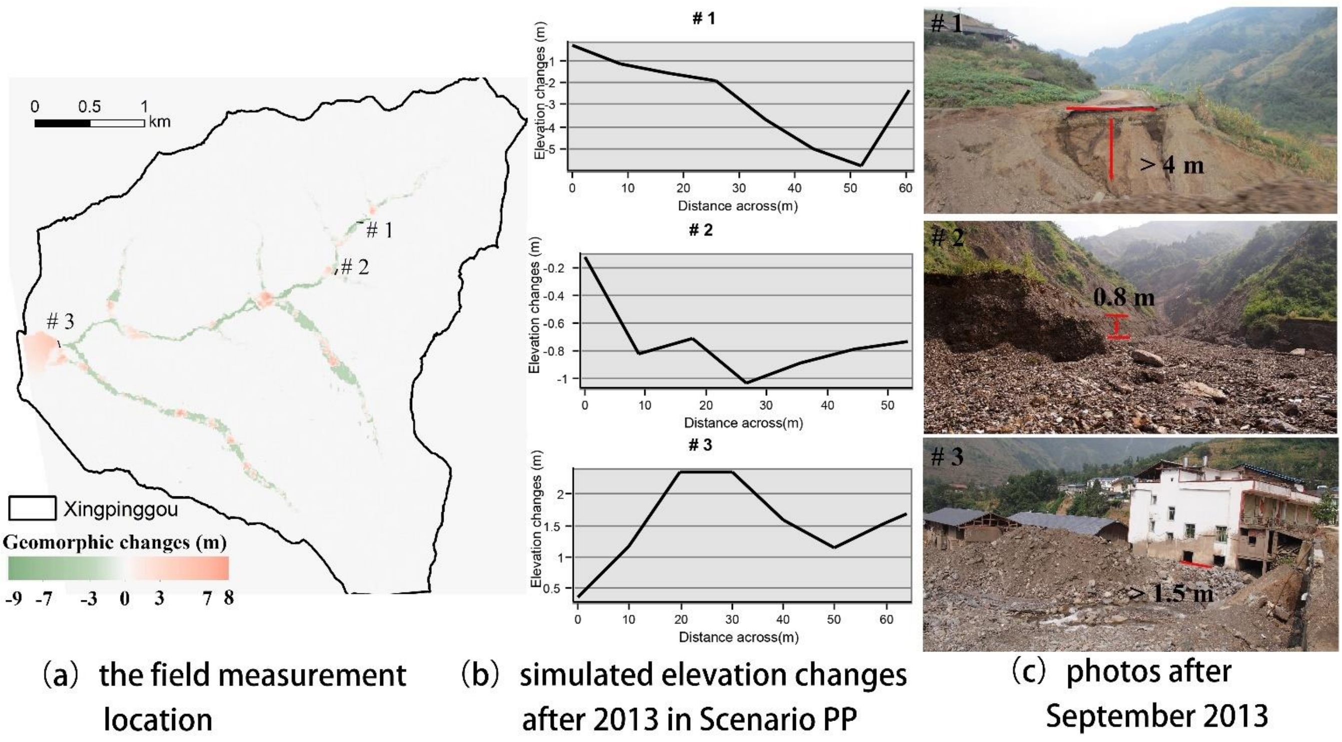

Figure 5: The comparison of cross-sections from the simulation results to the field measurements after 2013 in Scenario PP.

4.2 Overall geomorphic changes

Fig. 6a compares the three annual landscapes changes in each scenario, which were classified into nine categories by natural breaks for EleDiffs: extreme erosion (<-7 m), heavy erosion (-7--3 m), moderate erosion (-3--1 m), light erosion (1-0.1 m), micro change (-0.1-0.1 m), light deposition (0.1-1 m), moderate deposition (1-3 m), heavy deposition (3-7 m), and extreme deposition (>7 m). A similar spatial pattern of erosion is observed in all three scenarios. More specifically, erosion mainly occurred in the main channel and the branch valleys, among which the left branches were more severe. In contrast, the deposition distribution appeared to be varied in three scenarios, especially the area behind the two dams shown in Scenario PP and EP.

The total area of affected grid cells representing erosion and deposition in each scenario was calculated to reveal the difference (Fig. 6b). The affected area in Scenario UP was the largest at about 0.76 km^2 (5.4% of the total catchment), which was larger than that in Scenario PP (0.70 km^2, 5.0% of the whole catchment), and the affected area decreased to 0.61 km^2 (4.4% of the total catchment) in Scenario EP. The total area of erosion and deposition reduced gradually with more controlling measures established in this study.

Fig. 6c compares the extent of geomorphic changes in three situations using the areas varied in depth. The light and moderate erosion areas were more than the extreme and heavy ones for all three scenarios. The size of each erosion degree in UP was more extensive than in PP and followed by EP. In addition, the greater the deposition depth, the less deposition coverage. Especially the extreme deposition area was somewhat more than the area of the heavy deposition in UP. Further analysis shows that extreme, moderate, and light deposition areas decreased in the order of UP, PP, and EP. The heavy deposition areas show the opposite trend, mainly attributed to the checking dams and vegetation revetments.

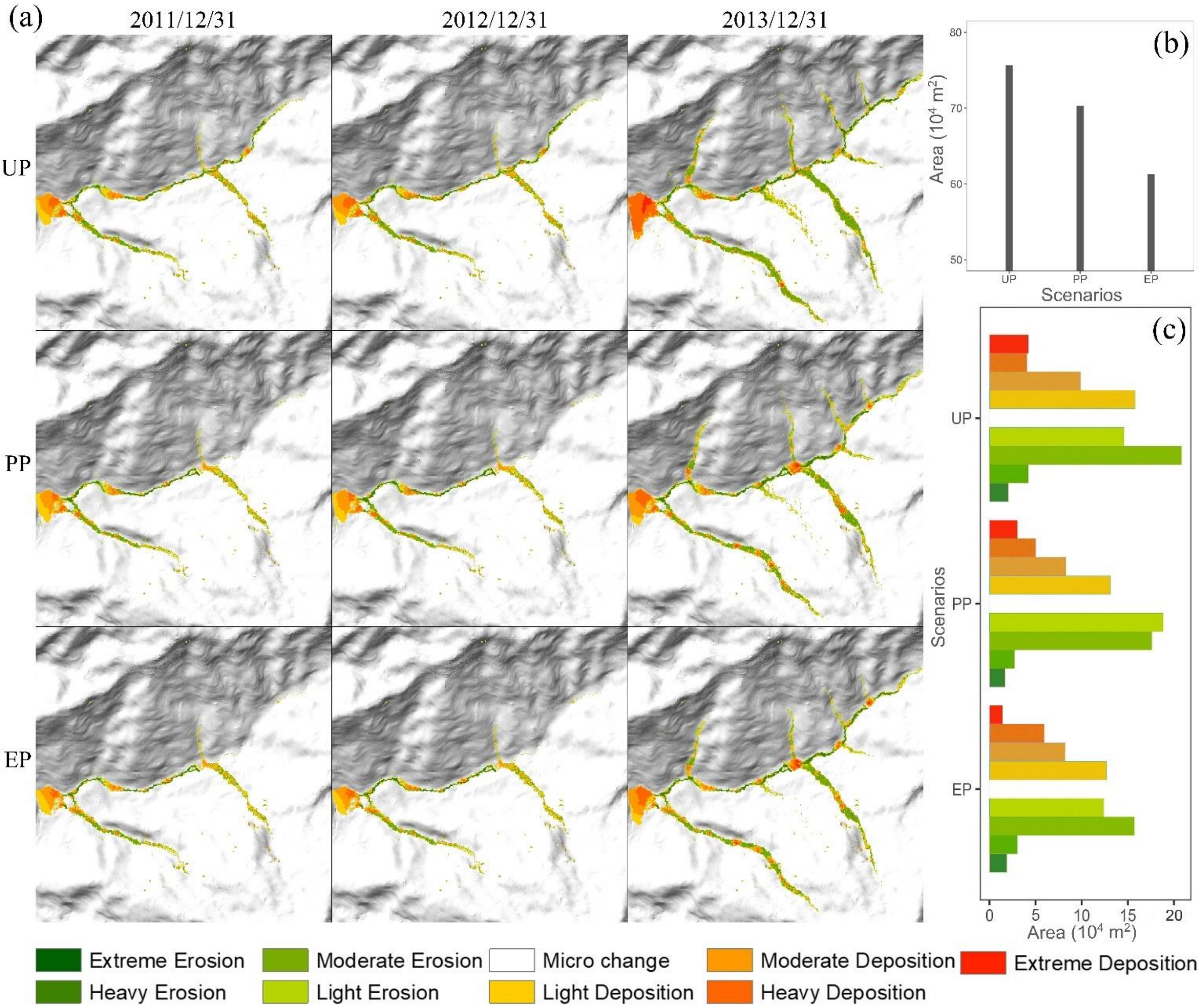

Figure 6: (a) Simulated geomorphic changes over time for three scenarios; (b) the affected area of deposition and erosion for three scenarios; (c) columnar distribution of different erosion and deposition levels.

4.3 Details of key spots

As shown in Fig. 7, the controlling measures and surroundings for the three scenarios were further investigated. Behind the two dams upriver, the evident orange clusters indicate that the deposition occurred in Scenario PP and EP. In contrast, these locations were dominated by erosion, shown in green in scenario UP. Further analysis of the sediment depth shown in Fig. 8 showed that the deposited depth behind the dams in Scenario EP was lower than those in Scenario PP. Additionally, in Scenario PP, sediment trapped by dam 1 was less than that by dam 2, but both have deposit thicknesses of more than 10 m, which exceeded the dams' heights (dam 1's height is 10 m, dam 2's height is 9 m). As for the simulation results in Scenario EP, the values of deposition depth behind the two dams were nearly 8 m, which were lower than the dams' heights.

The material produced from upriver tributary gullies varied due to the additional biological protection measures in three scenarios. A volume of 14.4×10^4 m^3 sediments was transported from EP's biological protection area (solid lines in Fig. 7). 27.1×10^4 m^3 and 16.9×10^4 m^3 loose material were produced in the same region without biological protection in Scenario UP and PP, respectively. The vegetation revetment enhanced the sediment conservation based on the role of dam 1. Compared with the deposition in UP and PP without levees in the downriver area (shown in the bottom row of Fig. 7), the levees in EP blocked debris in the bend of the channel and played an essential role in protecting the residents and cultivated land behind the levees.

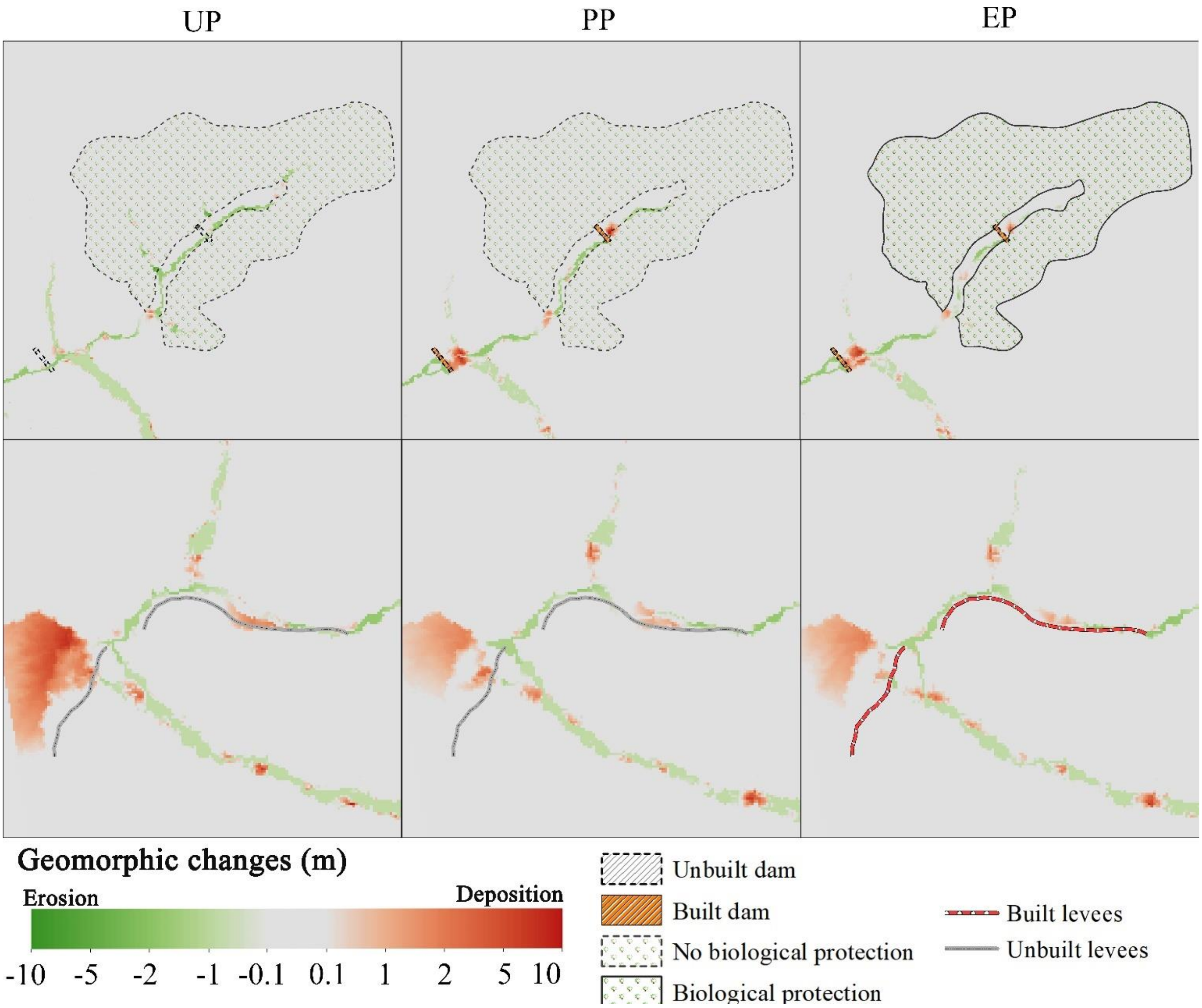

Figure 7: Geomorphic changes at key spots of the simulation results for the UP, PP, and EP scenarios. The top row is the upriver extent containing dam 1, dam 2 and the vegetation revetment. The bottom row is the downriver extent containing levees.

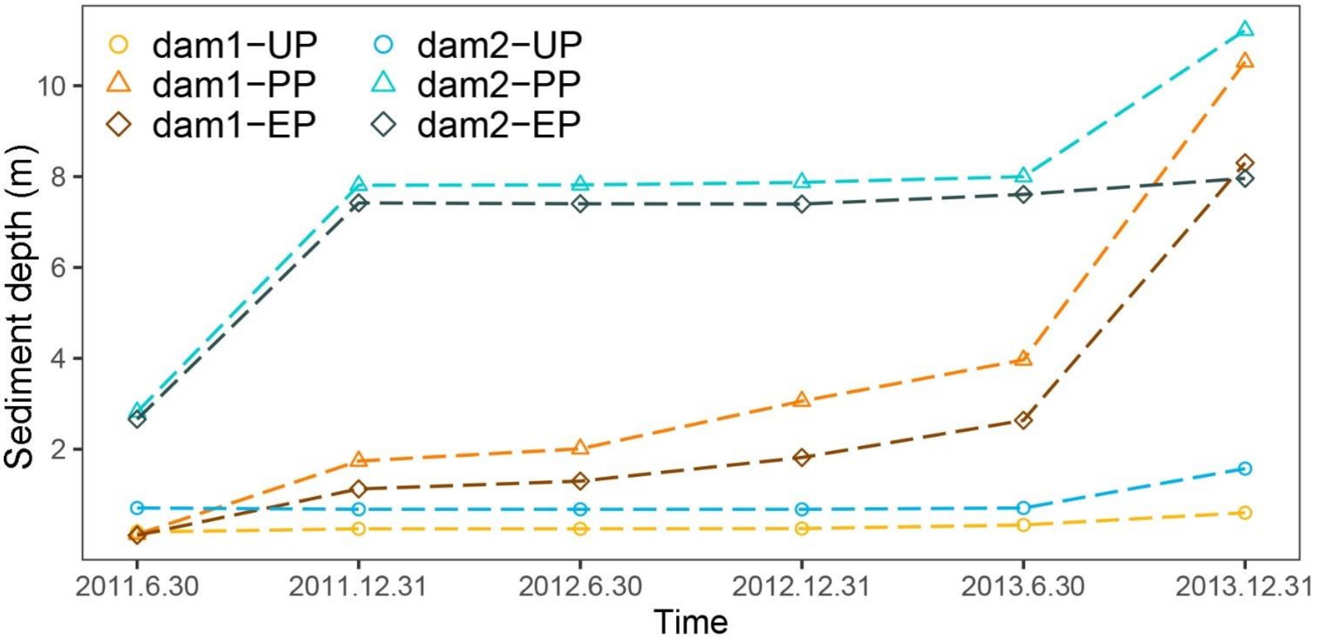

Figure 8: The depth of deposited sediment in the dams' placements.

4.4 Effectiveness assessment of intervention measures

Fig. 9 shows the erosion and deposition volumes in the source, transitional, and deposit areas and compares conservation ability (*Ca*) in each scenario. For all three scenarios, the deposition volume in the source area was less than that in the transitional area, and the largest amount of sediment was deposited in the deposit area. Regarding the eroded sediment, the largest volume was in the transitional area, followed by the transitional area, and the source area presented the least volume. Moreover, sediment transport was best controlled in the deposit area and worst contained in the source area under any intervention conditions.

Compared with the *Ca* of the source area in Scenario UP, the value was increased by 138.1% in Scenario PP, which was attributed to the dam1. Likewise, dam 2 in the transitional area reduced sediment loss effectively, which was reflected by a 52.5% increase in *Ca*. Furthermore, the mitigation measures in Scenario PP with vegetation revetment and levees in Scenario EP worked better. The conservation ability in the source area increased by 161.9% due to the dam retainment and vegetation revetment, and the levees helped increase by 3.49% in the deposit area.

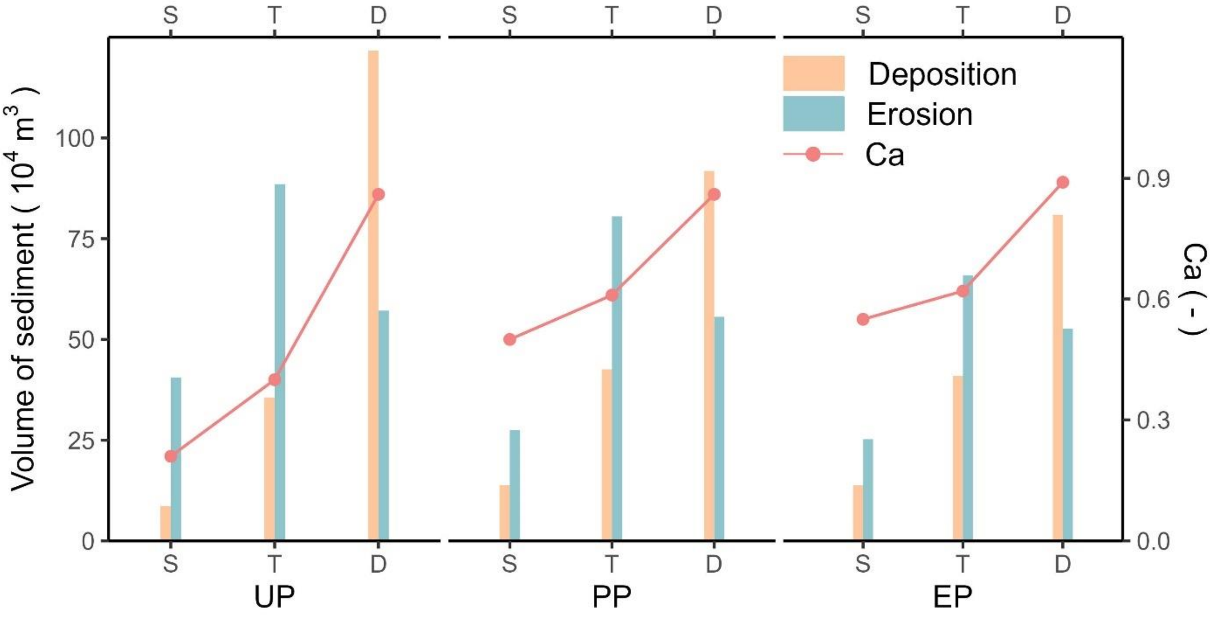

Figure 9: The volumes of sediment and the conservation ability (*Ca*) in three areas for each scenario (S: source area; T: transitional area; D: deposit area.).

The cumulative sediment yield time series for each scenario and the relative efficiency of scenario UP and EP are present in Fig. 10b and Fig. 10a, respectively. The steep curve of output cumulative sediment means a significant increase in the deposition. Three increasing stages are consistent with the rainfall intensity in three monsoons (May-September). The total sediment output in UP was the largest of ~30.4×10^4 m^3, followed by sediment yield in PP (26.3×10^4 m^3), and EP presented the least figure (19.3×10^4 m^3).

The relative efficiency over the period of controlling measures by human intervention in PP and EP (Fig. 10b) indicates three distinct stages. Stage I shows that the intervention measures in both scenarios prevented the sediment transport completely. Later stage II is a peculiar period when the effect of enhanced protective measures in EP was not as good as that in PP through repeated experiments. For stage III, the relative efficiency of the intervention measures in EP was greater than that in UP for a more prolonged stage III, which could achieve the long-term effect and stable conservation of solid material.

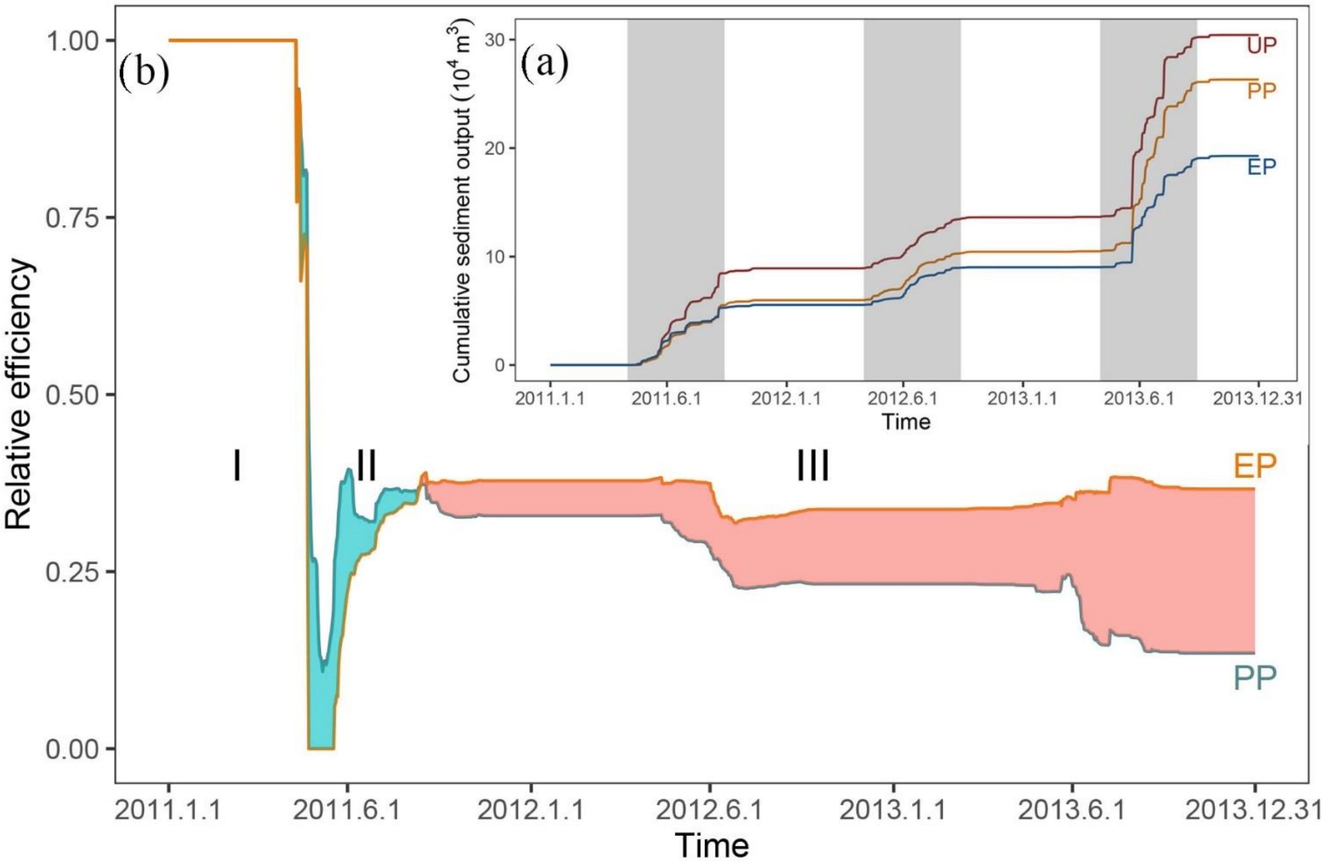

Figure 10: (a) cumulative sediment yield over time (grey region highlighting three monsoons), (b) relative efficiency of scenario UP and EP compared with the UP (cyan shading represents when PP is more effective than EP and red shading represents the opposite)

5. Discussion

5.1 Model calibration and uncertainty

The calibration and uncertainty are essential issues in the CAESAR-Lisflood (C-L) simulation of the geomorphic response to intervention measures (Yeh and Li, 2006). A preliminary calibration was carried out by replicating the geomorphic changes and water depth driven by an extreme rainfall event that occurred in 2018. The results (Fig. S3) demonstrated that the C-L successfully replicated the flash flood event using the initial conditions and model parameters. Actually, the calibration of the replicating ability of the geomorphic response to intervention measures was derived from a direct comparison between model results and direct measurements (Fig. 4 and Fig. 5). As a result, the simulated water discharge was more than the measured one but with the same order of magnitude. Moreover, the errors of erosion and deposition depth between simulation in Scenario PP and photographic evidence in three locations were at most 20%. The results suggest the robustness of the model settings and parameterisation.

The source of uncertainty is mainly from the model parameters and driving factors. Skinner et al. (2018b) provided a detailed sensitivity analysis of C-L, indicating that the sediment transport formula significantly influences a smaller catchment modelled by 10 m-grid cells. The sediment transport law, Wilcock and Crowe equations (Wilcock et al., 2003) have been proven suitable in the Xingping valley (Xie et al., 2018, 2022a, b; Li et al., 2020). Nevertheless, the empirical models of sediment transport would overpredict bedload transport rates in steep streams (gradients greater than 3%) (D'Agostino and Lenzi, 1999; Yager et al., 2012). Additionally, the driving factor, the input hourly rainfall data downscaled from the daily sequence is an unrealistic situation. Various sediment transport equations and downscaled hourly rainfall data need to be tested in C-L to determine the uncertainty further.

5.2 Intervention effects

The more facilities equivalent to more comprehensive intervention systems in this study aim to control sediment delivery. The C-L simulation of the geomorphic response to intervention measures suggests considerable influence on spatial modification and sediment yield. The relative systematic measures lead to fewer total affected areas (7.9%-19.7%) and sediment yield (16.7%~36.7%), which are suggested in overall evidence (see Fig. 6 and Fig. 10). Such catchment-scale performance disturbed by the extreme event is in line with the viewpoints of other authors (Chen et al., 2023; Lan et al., 2020; Chen et al., 2015).

The mitigation measures considerably changed the soil conservation ability in three sub-regions, especially in the source area. Herein, two main reasons why the erosion material is less in the source area than in another two sub-regions are inferred from the interactions of loose material and topographic constraints. First, the abundant loose solid material formed by the strong earthquake have stabilised overall since 2008's debris flow (details in Table S1). Second, the long and deep gullies are mainly located in the transitional area (Yaogouli, Shicouzi, Yangjiashan) and deposit area (Qinggangping), which provide more sediment supply than the source area. As shown in Fig. S4, the movement of the material occurred mainly in the branch valleys in the transitional and deposit area.

Moreover, comparing details and conservation ability with three scenarios stressed the unique role played by different intervention measures. For example, the check dams are most effective in blocking sediment, and the vegetation revetments strengthen the conservation ability. The synergy effect of soil conservation ability of checks dams and vegetable coverage is created with an increase of more than two times. The levees are barriers with a discernable impact on sediment conservation but with a special specific object-oriented protection.

The effectiveness of mitigation measures detected will decrease over time with a smaller downward trend. We supplement a ten-year experiment to reveal the decreasing trend over a more extended period. We randomly selected one of the 50 repeated rainfall datasets (year 2016-year 2025) downscaled by Li et al., 2020, which were generated from NEX-GDDP product (spatial resolution: 0.25°×0.25°, temporal resolution: daily) under RCP 4.5 emission scenario. The extracted rainfall sequence was then input to C-L to simulate the effectiveness of three intervention scenarios. The result (Fig. 11) illustrates that stage III (the stable stage that started on the 161st day, in which Scenario EP's intervention measures were more effective) lasted longer than stages I and II, which were only at the start. The relative effectiveness in both PP and EP scenarios decreased gradually, while the curve fell faster in PP than in EP.

The storage capacity of checking dams fades as the accumulation of sediment deposits, which necessarily lead to the gradual decrease of intervention effectiveness. Additionally, the vegetation revetments remain operationally effective in reducing sediment transport by stabilising topsoil over the period when the role of dam reservoirs gradually fails due to the lack of dredging work. Therefore, the vegetation protection strategy is vital for “green development” to reduce sediment loss but requires further efforts.

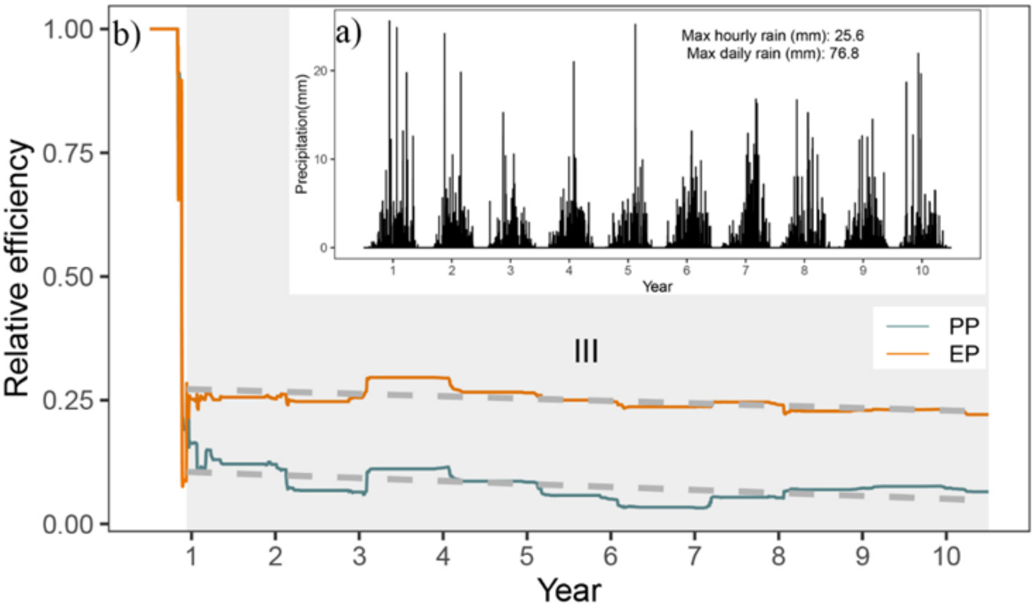

Figure 11: Future rainfall input and relative efficiency of sediment intervention measures. (a) rainfall downscaled from stochastic future rain; (b) the relative efficiency changes over ten years (grey region highlighting stage III, and the grey dashed lines indicating the linear fitting curve).

5.2 Limitations and applications

We built the dams and levees in our simulations by increasing the elevation in the expected location and assuming that it could not be eroded (see https://sourceforge.net/projects/caesar-lisflood/). This method proved experimentally feasible (Poeppl et al., 2019; Gioia and Schiattarella, 2020). The rigid dam and levee body embedded in the model would not be broken or weakened over time so the simulation result could underestimate the geo-hazard risk. Considering the complexity of the geo-hazard mechanism, the abovementioned tools could not simulate the occurring process of geo-hazard chain links. They would ignore the fierce attack on the environment and facilities downstream. Some typical geo-hazard chains were focused on the specified event in a short time and recreated the hazard lifecycle using physical and mechanical models (Fan et al., 2020).

The methods applied in the study further demonstrate that C-L is an effective tool for understanding the short-medium term or long-term geomorphology changes (Ramirez et al., 2022; Li et al., 2020; Coulthard et al., 2012a) and observing the effectiveness of natural hazard interventions measures under different rainfall patterns. Our simulations indicate that the mitigation facilities in this study were effective, especially engineering efforts cooperating with vegetation revetments in the upstream area, which would help decision-makers to optimise the management strategies to control mountain disasters. Geotechnical engineering has disadvantages, even though it is a mature technology that identifies and fixes problems quickly (Cui and Lin, 2013), such as the greater work and expense and the difficulty of maintenance. While the “green development”, the vegetation cover was effective in preventing erosion by strengthening topsoil and absorbing excess rainwater with its roots (Reichenbach et al., 2014; Stokes et al., 2014; Forbes and Broadhead, 2013; Mickovski et al., 2007). Alternatively, the methods could be used to study the tree planting patterns on different slopes.

6. Conclusions

In this study, the scenarios intervented by check dams, biological measures and artificial barriers are simulated using the C-L to outline the erosion and deposition area, measure the impacts of blocking sediment, and examine how the vegetable revetments helped to stabilise the slope. Four key findings are concluded. First, the engineering measures in controlling sediment transport are efficient, and the performance in protecting the fragile environment would be improved combined with other intervention measures like vegetation revetment and artificial barriers. Second, the effectiveness of mitigation measures would decrease over time. Third, the characteristics of sediment transport patterns changed considerably caused of the intervention measures. The stabilising sediment ability in the source area increased by 161.9% with the additional effect of vegetation revetments. At last, the present intervention measures are inadequate to reduce erosion and should be combined with dredging work.

Declaration of interest statement

The authors declare that they have no known competing financial interests or personal relationships that could have appeared to influence the work reported in this paper.

Author contribution

Di Wang: Conceptualisation, Methodology, Software, Writing-original draft preparation. Ming Wang Kai Liu and Jun Xie: Supervision, Methodology, Writing- Reviewing and Editing, Validation.

Acknowledgements

This research was supported by the National Key Research and Development Plan (2017YFC1502902). The financial support is highly appreciated. The authors would also like to thank Professor Tom Coulthard and his team for their excellent work on the freely available C-L model (https://sourceforge.net/projects/ caesar-lisflood).

Reference

Bates, P. D., Horritt, M. S., and Fewtrell, T. J.: A simple inertial formulation of the shallow water equations for efficient two-dimensional flood inundation modelling, J. Hydrol., 387, 33–45, https://doi.org/10.1016/j.jhydrol.2010.03.027, 2010.

Batty, M. and Xie, Y.: Possible urban automata, Environ. Plan. B Plan. Des., 24, 175–192, https://doi.org/10.1068/b240175, 1997.

Beven, K.: Linking parameters across scales: subgrid parameterizations and scale dependent hydrological models, Hydrol. Process., 9, 507–525, https://doi.org/https://doi.org/10.1002/hyp.3360090504, 1995.

Beven, K.: TOPMODEL:A critical, Hydrol. Process., 11, 1069–1085, https://doi.org/https://doi.org/10.1002/(SICI)1099-1085(199707)11:9<1069::AID-HYP545>3.0.CO;2-O, 1997.

Beven, K. J. and Kirkby, M. J.: A physically based, variable contributing area model of basin hydrology, Hydrol. Sci. Bull., 24, 43–69, https://doi.org/10.1080/02626667909491834, 1979.

Chen, N., Zhou, H., Yang, L., Yang, L., and Lv, L.: Analysis of benefits of debris flow control projects in southwest mountains areas of China, J. Chengdu Univ. Technol. (Science Technol. Ed., 40, 50–58, https://doi.org/10.3969/j.issn.1671-9727.2013.01.008, 2013.

Chen, X., Li, Z., Cui, P., and Liu, X.: Estimation of soil erosion caused by the 5.12 Wenchuan Earthquake, J. Mt. Sci., 27, 122–127, 2009.

Chen, X., Cui, P., You, Y., Chen, J., and Li, D.: Engineering measures for debris flow hazard mitigation in the Wenchuan earthquake area, Eng. Geol., 194, 73–85, https://doi.org/10.1016/j.enggeo.2014.10.002, 2015.

Chen, Y., Li, J., Jiao, J., Wang, N., Bai, L., Chen, T., Zhao, C., Zhang, Z., Xu, Q., and Han, J.: Modeling the impacts of fully-filled check dams on flood processes using CAESAR-lisflood model in the Shejiagou catchment of the Loess Plateau, China, J. Hydrol. Reg. Stud., 45, 101290, https://doi.org/10.1016/j.ejrh.2022.101290, 2023.

Cong, K., Li, R., and Bi, Y.: Benefit evaluation of debris flow control engineering based on the FLO-2D model, Northwest. Geol., 52, https://doi.org/10.19751/j.cnki.61-1149/p.2019.03.019, 2019.

Couclelis, H.: From cellular automata to urban models: new principles for model development and implementation, Environ. Plan. B Plan. Des., 24, 165–174, https://doi.org/10.1068/b240165, 1997.

Coulthard, T. J. and Skinner, C. J.: The sensitivity of landscape evolution models to spatial and temporal rainfall resolution, Earth Surf. Dyn., 4, 757–771, https://doi.org/10.5194/esurf-4-757-2016, 2016.

Coulthard, T. J. and Wiel, Van De J., M.: Modelling long term basin scale sediment connectivity, driven by spatial land use changes, Geomorphology, 277, 265–281, https://doi.org/10.1016/j.geomorph.2016.05.027, 2017.

Coulthard, T. J., Macklin, M. G., and Kirkby, M. J.: A cellular model of Holocene upland river basin and alluvial fan evolution, Earth Surf. Process. Landforms, 27, 269–288, https://doi.org/10.1002/esp.318, 2002.

Coulthard, T. J., Hancock, G. R., and Lowry, J. B. C.: Modelling soil erosion with a downscaled landscape evolution model, Earth Surf. Process. Landforms, 37, 1046–1055, https://doi.org/10.1002/esp.3226, 2012a.

Coulthard, T. J., Ramirez, J., Fowler, H. J., and Glenis, V.: Using the UKCP09 probabilistic scenarios to model the amplified impact of climate change on drainage basin sediment yield, Hydrol. Earth Syst. Sci., 16, 4401–4416, https://doi.org/10.5194/hess-16-4401-2012, 2012b.

Coulthard, T. J., Neal, J. C., Bates, P. D., Ramirez, J., de Almeida, G. A. M., and Hancock, G. R.: Integrating the LISFLOOD-FP 2D hydrodynamic model with the CAESAR model: Implications for modelling landscape evolution, Earth Surf. Process. Landforms, 38, 1897–1906, https://doi.org/10.1002/esp.3478, 2013.

Cui, P. and Lin, Y.: Debris-Flow Treatment: The Integration of Botanical and Geotechnical Methods, J. Resour. Ecol., 4, 097–104, https://doi.org/10.5814/j.issn.1674-764x.2013.02.001, 2013.

Cui, P., Zhou, G. G. D., Zhu, X. H., and Zhang, J. Q.: Scale amplification of natural debris flows caused by cascading landslide dam failures, Geomorphology, 182, 173–189, https://doi.org/10.1016/j.geomorph.2012.11.009, 2013.

D’Agostino, V. and Lenzi, M. A.: Bedload transport in the instrumented catchment of the Rio Cordon. Part II: Analysis of the bedload rate, Catena, 36, 191–204, https://doi.org/10.1016/S0341-8162(99)00017-X, 1999.

Einstein, H. A.: The Bed-Load Function for Sediment Transportation in Open Channel Flows, 1950.

Fan, X., Yang, F., Siva Subramanian, S., Xu, Q., Feng, Z., Mavrouli, O., Peng, M., Ouyang, C., Jansen, J. D., and Huang, R.: Prediction of a multi-hazard chain by an integrated numerical simulation approach: the Baige landslide, Jinsha River, China, Landslides, 17, 147–164, https://doi.org/10.1007/s10346-019-01313-5, 2020.

Feng, W., He, S., Liu, Z., Yi, X., and Bai, H.: Features of Debris Flows and Their Engineering Control Effects at Xinping Gully of Pingwu County, J. Eng. Geol., 25, https://doi.org/10． 13544 / j． cnki． jeg． 2017． 03． 027, 2017.

Forbes, K. and Broadhead, J.: Forests and landslides: the role of trees and forests in the prevention of landslides and rehabilitation of landslide-affected areas in Asia, FAO, 14–18 pp., 2013.

Gioia, D. and Schiattarella, M.: Modeling Short-Term Landscape Modification and Sedimentary Budget Induced by Dam Removal: Insights from LEM Application, Appl. Sci., 10, 7697, https://doi.org/10.3390/app10217697, 2020.

Goldberg, D. E.: Genetic Algorithms in Search, Optimization, and Machine Learning, Addison-Wesley Longman Publishing Co., Inc., 372 pp., https://doi.org/10.1007/BF01920603, 1989.

Gorum, T., Fan, X., van Westen, C. J., Huang, R. Q., Xu, Q., Tang, C., and Wang, G.: Distribution pattern of earthquake-induced landslides triggered by the 12 May 2008 Wenchuan earthquake, Geomorphology, 133, 152–167, https://doi.org/10.1016/j.geomorph.2010.12.030, 2011.

Guo, Q., Xiao, J., and Guan, X.: The characteristics of debris flow activities and its optimal timing for the control in Shikan River Basin Pingwu Country, Chinese J. Geol. Hazard Control, 29, https://doi.org/10. 16031/j. cnki. issn. 1003-8035. 2018. 03. 05, 2018.

Hancock, G. R., Verdon-Kidd, D., and Lowry, J. B. C.: Soil erosion predictions from a landscape evolution model – An assessment of a post-mining landform using spatial climate change analogues, Sci. Total Environ., 601–602, 109–121, https://doi.org/10.1016/j.scitotenv.2017.04.038, 2017.

He, J., Zhang, L., Fan, R., Zhou, S., Luo, H., and Peng, D.: Evaluating effectiveness of mitigation measures for large debris flows in Wenchuan, China, Landslides, 19, 913–928, https://doi.org/10.1007/s10346-021-01809-z, 2022.

Huang, R.: Geohazard assessment of the Wenchuan earthquake, Science Press, Beijing, 944 pp., 2009.

Huang, R. and Fan, X.: The landslide story, Nat. Geosci., 6, 325–326, https://doi.org/10.1038/ngeo1806, 2013.

J.B.C. Lowry, M. Narayan, G.R. Hancock, and K.G. Evans: Understanding post-mining landforms:Utilising pre-mine geomorphology to improve rehabilitation outcomes, Geomorphology, 328, 93–107, https://doi.org/10.1016/j.geomorph.2018.11.027, 2019.

Lan, H., Wang, D., He, S., Fang, Y., Chen, W., Zhao, P., and Qi, Y.: Experimental study on the effects of tree planting on slope stability, Landslides, 17, 1021–1035, https://doi.org/10.1007/s10346-020-01348-z, 2020.

Lee, T. and Jeong, C.: Nonparametric statistical temporal downscaling of daily precipitation to hourly precipitation and implications for climate change scenarios, J. Hydrol., 510, 182–196, https://doi.org/10.1016/j.jhydrol.2013.12.027, 2014.

Li, C., Wang, M., and Liu, K.: A decadal evolution of landslides and debris flows after the Wenchuan earthquake, Geomorphology, 323, 1–12, https://doi.org/10.1016/j.geomorph.2018.09.010, 2018.

Li, C., Wang, M., Liu, K., and Coulthard, T. J.: Landscape evolution of the Wenchuan earthquake-stricken area in response to future climate change, J. Hydrol., 590, 125244, https://doi.org/10.1016/j.jhydrol.2020.125244, 2020.

Marchi, L., Comiti, F., Crema, S., and Cavalli, M.: Channel control works and sediment connectivity in the European Alps, Sci. Total Environ., 668, 389–399, https://doi.org/10.1016/j.scitotenv.2019.02.416, 2019.

Mickovski, S. B., Bengough, A. G., Bransby, M. F., Davies, M. C. R., Hallett, P. D., and Sonnenberg, R.: Material stiffness, branching pattern and soil matric potential affect the pullout resistance of model root systems, Eur. J. Soil Sci., 58, 1471–1481, https://doi.org/10.1111/j.1365-2389.2007.00953.x, 2007.

Poeppl, R. E., Coulthard, T., Keesstra, S. D., and Keiler, M.: Modeling the impact of dam removal on channel evolution and sediment delivery in a multiple dam setting, Int. J. Sediment Res., 34, 537–549, https://doi.org/10.1016/j.ijsrc.2019.06.001, 2019.

Ramirez, J. A., Zischg, A. P., Schürmann, S., Zimmermann, M., Weingartner, R., Coulthard, T., and Keiler, M.: Modeling the geomorphic response to early river engineering works using CAESAR-Lisflood, Anthropocene, 32, https://doi.org/10.1016/j.ancene.2020.100266, 2020.

Ramirez, J. A., Mertin, M., Peleg, N., Horton, P., Skinner, C., Zimmermann, M., and Keiler, M.: Modelling the long-term geomorphic response to check dam failures in an alpine channel with CAESAR-Lisflood, Int. J. Sediment Res., 37, 687–700, https://doi.org/10.1016/j.ijsrc.2022.04.005, 2022.

Reichenbach, P., Busca, C., Mondini, A. C., and Rossi, M.: The Influence of Land Use Change on Landslide Susceptibility Zonation: The Briga Catchment Test Site (Messina, Italy), Environ. Manage., 54, 1372–1384, https://doi.org/10.1007/s00267-014-0357-0, 2014.

Saynor, M. J., Lowry, J. B. C., and Boyden, J. M.: Assessment of rip lines using CAESAR-Lisflood on a trial landform at the Ranger Uranium Mine, L. Degrad. Dev., 30, 504–514, https://doi.org/10.1002/ldr.3242, 2019.

Skinner, C. J., Coulthard, T. J., Schwanghart, W., Van De Wiel, M. J., and Hancock, G.: Global sensitivity analysis of parameter uncertainty in landscape evolution models, Geosci. Model Dev., 11, 4873–4888, https://doi.org/10.5194/gmd-11-4873-2018, 2018a.

Skinner, C. J., Coulthard, T. J., Schwanghart, W., Van De Wiel, M. J., and Hancock, G.: Global sensitivity analysis of parameter uncertainty in landscape evolution models, Geosci. Model Dev., 11, 4873–4888, https://doi.org/10.5194/gmd-11-4873-2018, 2018b.

Slingerland, N., Beier, N., and Wilson, G.: Stress testing geomorphic and traditional tailings dam designs for closure using a landscape evolution model, in: Proceedings of the 13th International Conference on Mine Closure, 1533–1544, https://doi.org/10.36487/ACG_rep/1915_120_Slingerland, 2019.

Stokes, A., Douglas, G. B., Fourcaud, T., Giadrossich, F., Gillies, C., Hubble, T., Kim, J. H., Loades, K. W., Mao, Z., McIvor, I. R., Mickovski, S. B., Mitchell, S., Osman, N., Phillips, C., Poesen, J., Polster, D., Preti, F., Raymond, P., Rey, F., Schwarz, M., and Walker, L. R.: Ecological mitigation of hillslope instability: Ten key issues facing researchers and practitioners, Plant Soil, 377, 1–23, https://doi.org/10.1007/s11104-014-2044-6, 2014.

Thomson, H. and Chandler, L.: Tailings storage facility landform evolution modelling, in: Proceedings of the 13th International Conference on Mine Closure, 385–396, https://doi.org/10.36487/ACG_rep/1915_31_Thomson, 2019.

Wang, M., Yang, W., Shi, P., Xu, C., and Liu, L.: Diagnosis of vegetation recovery in mountainous regions after the wenchuan earthquake, IEEE J. Sel. Top. Appl. Earth Obs. Remote Sens., 7, 3029–3037, https://doi.org/10.1109/JSTARS.2014.2327794, 2014a.

Wang, M., Liu, M., Yang, S., and Shi, P.: Incorporating Triggering and Environmental Factors in the Analysis of Earthquake-Induced Landslide Hazards, Int. J. Disaster Risk Sci., 5, 125–135, https://doi.org/10.1007/s13753-014-0020-7, 2014b.

Wang, N., Han, B., Pang, Q., and Yu, Z.: post-evaluation model on effectiveness of debris flow control, J. Eng. Geol., 23, 219–226, https://doi.org/10.13544/j.cnki.jeg.2015.02.005, 2015.

Van De Wiel, M. J., Coulthard, T. J., Macklin, M. G., and Lewin, J.: Embedding reach-scale fluvial dynamics within the CAESAR cellular automaton landscape evolution model, Geomorphology, 90, 283–301, https://doi.org/10.1016/j.geomorph.2006.10.024, 2007.

Wilcock, P. R., Asce, M., and Crowe, J. C.: Surface-based Transport Model for Mixed-Size Sediment Surface-based Transport Model for Mixed-Size Sediment, 9429, https://doi.org/10.1061/(ASCE)0733-9429(2003)129, 2003.

Xie, J., Wang, M., Liu, K., and Coulthard, T. J.: Modeling sediment movement and channel response to rainfall variability after a major earthquake, Geomorphology, 320, 18–32, https://doi.org/10.1016/j.geomorph.2018.07.022, 2018.

Xie, J., Coulthard, T. J., and McLelland, S. J.: Modelling the impact of seismic triggered landslide location on basin sediment yield, dynamics and connectivity, Geomorphology, 398, 108029, https://doi.org/10.1016/j.geomorph.2021.108029, 2022a.

Xie, J., Coulthard, T. J., Wang, M., and Wu, J.: Tracing seismic landslide-derived sediment dynamics in response to climate change, Catena, 217, 106495, https://doi.org/10.1016/j.catena.2022.106495, 2022b.

Xu, C., Xu, X., Yao, X., and Dai, F.: Three (nearly) complete inventories of landslides triggered by the May 12, 2008 Wenchuan Mw 7.9 earthquake of China and their spatial distribution statistical analysis, Landslides, 11, 441–461, https://doi.org/10.1007/s10346-013-0404-6, 2014.

Yager, E. M., Turowski, J. M., Rickenman, D., and McArdell, B. W.: Sediment supply, grain protrusion, and bedload transport in mountain streams, Geophys. Res. Lett., 39, 1–5, https://doi.org/10.1029/2012GL051654, 2012.

Yang, Z., Duan, X., Huang, J., Dong, Y., Zhang, X., Liu, J., and Yang, C.: Tracking long-term cascade check dam siltation: implications for debris flow control and landslide stability, Landslides, 18, 3923–3935, https://doi.org/10.1007/s10346-021-01755-w, 2021.

Yeh, A. G. O. and Li, X.: Errors and uncertainties in urban cellular automata, Comput. Environ. Urban Syst., 30, 10–28, https://doi.org/10.1016/j.compenvurbsys.2004.05.007, 2006.

Yu, B., Yang, Y., Su, Y., Huang, W., and Wang, G.: Research on the giant debris flow hazards in Zhouqu County, Gansu Province on August 7, 2010, J. Eng. Geol., 18, 437–444, https://doi.org/10.3969/j.issn.1004-9665.2010.04.001, 2010.

Zhang, L. and Liang, K.: Research on economic benefit evaluation of the prevention and cure project for debris flow, Chinese J. Geol. Hazard Control, 16, 48–53, https://doi.org/10.3969/j.issn.1003-8035.2005.03.011, 2005.

Zhang, X., Wang, M., Liu, K., Xie, J., and Xu, H.: Using NDVI time series to diagnose vegetation recovery after major earthquake based on dynamic time warping and lower bound distance, Ecol. Indic., 94, 52–61, https://doi.org/10.1016/j.ecolind.2018.06.026, 2018.

Zhou, H., Chen, N., Lu, Y., and Li, B.: Control Effectiveness of Check Dams in Debris Flow Gully: A Case of Huashiban Gully in Earthquake Worst-stricken Area，Beichuan County, J. Mt. Sci., 30, 347–354, https://doi.org/10.3969/j.issn.1008-2786.2012.03.015, 2012.